Quantification of D_2 Receptor Binding in the Rat Striatum Using Small Animal PET – The Impact of the Reference Tissue on the Binding Potential of [^{18}F]N-Methyl-Benperidol

Susanne Nikolaus[*,1], Rolf Larisch[2], Markus Beu[1], Henning Vosberg[1], Farhad Forutan[3], Andreas Wirrwar[1] and Hans-Wilhelm Müller[1]

[1]*Clinic of Nuclear Medicine, University Hospital Düsseldorf, Moorenstr. 5, D-40225 Düsseldorf, Germany*

[2]*Clinic of Nuclear Medicine, Clinic of Lüdenscheid, Paulmannshöherstr. 14, D-58515 Lüdenscheid, Germany*

[3]*Nuclear Medicine, Genovevastr. 24, D-51065 Köln, Germany*

Abstract: In the present study, the binding potential (BP) of the D_2 receptor radioligand [^{18}F]N-methyl-benperidol ([^{18}F]FMB) was determined with *in vivo* saturation binding analysis using either cerebellum or parietal cortex as reference region. For the purpose of validation, BP additionally was determined in the same set of animals by computing the equilibrium ratios of the distribution volumes (V_3''). With *in vivo* saturation binding analysis, the striatal BP as obtained with a cortical estimate for the free and non-specifically bound radioligand fell short of the BP as obtained with a cerebellar estimate by 70%. Similarly, with the equilibrium distribution volume method, the employment of a cortical REF led to a striatal V_3'', which was 30% lower than the V_3'' obtained with a cerebellar REF. The BP determined with *in vivo* saturation binding analysis and a cerebellar REF provided a closer approximation to the BP previously obtained with *in vitro* autoradiography relative to the BP determined with *in vivo* saturation binding analysis and a cortical REF. Findings show that *in vivo* saturation binding analysis is a feasible approach to obtain receptor binding parameters if scanner characteristics or other technical limitations preclude the kinetic modelling of binding data. However, caution should be exerted in choosing the reference tissue with regard to the intended investigation.

Keywords: [^{18}F]N-methyl-benperidol, dopamine D_2 receptors, small animal PET, *in vivo* saturation binding analysis.

INTRODUCTION

During the last decade, small animal positron emission tomography (PET) increasingly has been employed for the investigation of dopamine D_2 receptor binding in rat models of senescence, drug abuse, depression, attention-deficit hyperactivity disorder and neurodegenerative diseases including M. Parkinson and M. Huntington (for review see [1, 2]).

In PET investigations on humans, binding data are commonly analyzed applying the direct kinetic approach (for review see [3]). A prerequisite for this method is the measurement of the arterial free ligand concentration. Arterial input functions, however, are difficult to obtain in investigations performed on rat or mouse models, as sufficient amounts of blood may not repeatedly be drawn from animals of this small size. Moreover, the configuration as such of dedicated small animal PET scanners of the first generation (*e.g.* TierPET, RATPET, MADPET) precludes the kinetic modeling of data, as the initial radioligand uptake may not be measured with a sufficient temporal resolution. Typically, these scanners have a comparatively low sensitivity (10 to 40 cps/kBq; for review see [4]), which makes them merely suitable for a quasi-dynamic acquisition of data. Apart from limitations due to the scanner characteristics, PET investigations may be confounded by varying and low specific activities of the radiotracers possibly leading to the saturation of receptor binding. As a consequence, investigators must meet the challenge to elaborate reasonable compromises between the desirable and the feasible in small animal imaging.

In the small animal PET studies performed until now, the need for an arterial input function was obviated either by confinement to expressing radioactivity values as percentage of the injected dose per tissue volume [5], or by applying dynamic [6-8], non-invasive graphic [9-13], and simplified reference tissue models [12, 14-23]. We recently proposed the performance of *in vivo* saturation binding analysis of [^{18}F]N-methyl-benperidol ([^{18}F]FMB) binding to the D_2 receptors in the rat striatum [24-26]. One benefit of the saturation binding approach is that it allows the separate determination of receptor density (B_{max}) and the dissociation constant (K_d) as a measure of affinity. Moreover, this method per definition requires the saturation of receptor binding and, thus, the application of increasing radioligand concentrations. As a consequence, radiochemical syntheses delivering radioligands with low specific activities must not be discarded, but may even be used to advantage, when *in vivo* saturation binding analysis can be applied.

*Address correspondence to this author at the Clinic of Nuclear Medicine, University Hospital Düsseldorf, Moorenstr. 5, D-40225 Düsseldorf, Germany; Tel: 0049-(0)211-81-17048; Fax: 0049-(0)211-81-17041; E-mail: Susanne.Nikolaus@uni-duesseldorf.de

1876-388X/09

The *in vivo* saturation binding approach is based on the assumption that *in vitro* radioligand binding assays can be conceived as two-compartment systems with both compartments localized in the same test tube and representing the ligand-containing buffer solution and the receptor-containing tissue samples, respectively. In transferring the principle of autoradiographic evaluation to *in vivo* imaging methods, the free ligand concentration, [L], can be assigned to the pooled compartments $C_2 + C_2$', whereas the concentrations of unbound receptors, [R], and receptor-radioligand complexes, [LR], adhere to C_3. Specific binding, then, is the difference between total radioactivity concentrations, [LR], in the region of interest (ROI) and the non-specific and free radioactivity concentrations, [L], as measured in the reference region (REF). When [LR] is plotted against [L], B_{max} and K_d as *in vitro* saturation binding analysis may be derived from the resulting hyperbolic curve by non-linear or linear regression analysis with B_{max}/K_d as an estimation of the binding potential (BP).

For the purpose of validation, in the present study, BP additionally was determined in the same animals by computing the equilibrium ratio of the distribution volumes of the specifically and the non-specifically bound compartment ($V_3'' = V_3/V_2$) as an estimate for BP [27]. V_3'' can be obtained as $(V_T/V_2) - 1$, with V_T denoting the total tissue equilibrium volume of distribution, equal to the sum of V_2 and V_3. If it is assumed that the equilibrium concentrations of free and non-specifically bound ligand are the same across brain regions, V_2 may be inferred from a reference region (REF) devoid of the target receptor (*e.g.* cortex or cerebellum), and V_3'' in the striatum is obtained as $V_T(ROI)/V_T(REF) - 1$.

In all small animal PET and SPECT investigations using cerebral reference tissue for the quantification of specific D2 receptor radioligand binding, the cerebellum has been employed as a REF (for review see [1]). Matters, however, are different in clinical investigations of D_2 receptor binding, where cerebellar (*e.g.* [28-30]) and cortical REFs (*e.g.* [31-33]), have been used to the same extent. Autoradiographic studies on cerebral tissues of rats have shown that frontocortical and cerebellar D_2 receptor ligand accumulations amounted to 3 and 1%, respectively, of striatal binding [34]. Similarly, in humans, frontocortical and cerebellar D_2 receptor ligand accumulations fell short of striatal binding by 90 and a 98%, respectively [31].

These differences prompted us to additionally assess the influence of the chosen reference tissue on the BP of [^{18}F]FMB in the rat striatum obtained with either *in vivo* saturation binding analysis and the equilibrium distribution volume method.

MATERIALS AND METHODOLOGY

Animals

Eight male Sprague-Dawley rats (Charles River, France), weighing between 300 and 500 g were investigated with small animal PET. The study was approved by the regional authority; it was carried out in accordance with the National Institute of Health Guide for the Care and Use of Laboratory Animals (NIH Publications No. 80-23, rev. 1996 and and the German Law on the Protection of Animals.

Radiochemistry

[^{18}F]FMB was synthesized as previously described [35]. Nucleophilic aromatic fluorination *via* ^{18}F-for-nitro-exchange was performed according to the method described for the butyrophenone ligand [^{18}F](N-methyl)-spiperone [36]. The radiochemical purity was above 98% as determined with High Performance Liquid Chromatography. [^{18}F]FMB is rapidly metabolized in the periphery [37]. Thereby, chromatographic analysis suggests that only polar metabolites are formed, which do not partition into the brain [38]. Specific activity at injection time covered one order of magnitude (range: > 11 to > 100 TBq/mmol). The molar amounts of injected radioligand ranged from 0.81 to 0.54 nmol.

Acquisition of Imaging Data

Instrumentation. The small animal tomograph ("TierPET", Zentrallabor für Elektronik', Forschungszentrum Jülich GmbH, Jülich, Germany) was described in detail elsewhere [39]. Axial as well as transaxial field of view had a diameter of 40 mm. The resolution amounted to 2.1 mm (FWHM). One count/sec/mm³ as registered with the camera corresponded to 444 Bq/mm³ [40]; this value served as a calibration factor in order to calculate radioactivity concentrations from the count rates within the ROIs.

Protocol. After short-time inhalation anesthesia with isofluran, animals received intramuscular injections of ketamine (concentration: 100 mg/ml, dose: 0.9 ml/kg) and xylazine (concentration: 0.02 mg/ml, dose: 0.4 ml/kg). [^{18}F]FMB (70.4 ± 8.7 MBq; mean ± SD) was diluted in 0.9% saline containing 10% ethanol and injected into the right jugular vein. The mean injection volume was 1 ± 0.5 ml; the mean injected radioactivity dose amounted to 158.3 ± 24.2 MBq/kg.

Time-activity curves had shown that the equilibrium between radioactivity concentrations of specifically-bound and both non-specifically bound and free [^{18}F]FMB is reached at 20 min post-injection and remains stable for up to 3 hours [41]. In the present study, imaging data were acquired dynamically for 36 min (6 time frames of 6 min each) with angular steps of 7.5° (30 sec per angular step). The mean delay between application of the radioligand and start of the measurement amounted to 8.1 ± 4.4 min. The data processing was described in detail elsewhere [25, 26, 41]. Image reconstruction was performed in consecutive slices of 2 mm thickness.

Evaluation

Saturation binding analysis. Images were analyzed with the Multi Purpose Imaging Tool (version 2.57; Advanced Tomo Vision, Erftstadt, Germany). According to the standard rat brain atlas by Paxinos and Watson [42], striata and cerebellum were localized individually for each animal on coronal sections. Two standard circular ROIs with diameters of 2.5 mm were drawn around the centers of both striata. Within the cerebellum, a circular region with a diameter of 5.5 mm was delineated. The positions but not the sizes of the ROIs were adjusted individually for each animal by two operators, independently. The obtained radioactivity values were corrected for radioactive decay. As time-activity

curves had shown that the equilibrium between radioactivity concentrations of specifically-bound and both non-specifically bound and free [^{18}F]FMB was reached at 20 min post-injection, left and right radioactivity concentrations in time frames four to six were averaged according to the late-time method [43].

Previous investigations with the TierPET had shown that in a target with a diameter of 2.5 mm, radioactivity was underestimated by approximately 60% [40]. On the basis of these measurements partial volume corrections were perfomed for the striatum of each side.

Fig. (**1A**) shows a characteristic coronal slice of a rat head obtained with the PET camera with the highest radioactivity accumulations in Harderian glands and neostriatum. In order to estimate the various amounts of spill-over affecting striatal and cortical radioactivity concentrations, Gaussian model functions ($y = A_{HG} \exp(-0.5[(x-m_{HG})/s_{HG}]^2 + A_{STR} \exp(-0.5[(x-m_{STR})/s_{STR}]^2 + A_{COR} \exp(-0.5[(x-m_{COR})/s_{COR}]^2$ were fitted to line-activity profiles through Harderian gland, striatum and adjacent cortex with A_{HG}, A_{STR} and A_{COR} as peak heights, m_{HG}, m_{STR} and m_{COR} as the x-coordinates of the peaks and s_{HG}, s_{STR} and s_{COR} as the FWHM values of glandular, striatal and cortical curves. After decomposition of the sum function into a glandular, striatal and cortical portion, the amount of spill-over was determined by relating the integrals of the overlaps to the integrals of the curves (Fig. **1B**). The percentual contributions of one curve to another were subtracted for each side from the striatal radioactivity concentrations.

Either cortical radioactivity - as inferred from the line-activty profiles - or cerebellar radioactivity was considered as an estimate of the free and non-specifically bound radioligand in brain tissue. From striatal, cortical and cerebellar radioactivity concentrations (MBq/mm³) and the known specific activity at the beginning of the fourth time frame, striatal, cortical and cerebellar molar radioligand concentrations (fmol/mg) were calculated. For each animal, either cortical or cerebellar molar concentrations were subtracted from left and right striatal radioligand concentrations in order to obtain specific binding. For left and right striatum specific binding was averaged. The results obtained with cortical radioactivity as an estimate of the free and non-specifically bound radioligand have been previously published [24].

For non-linear regression analysis (GraphPad Prism, GraphPad Software, San Diego, USA), saturation binding

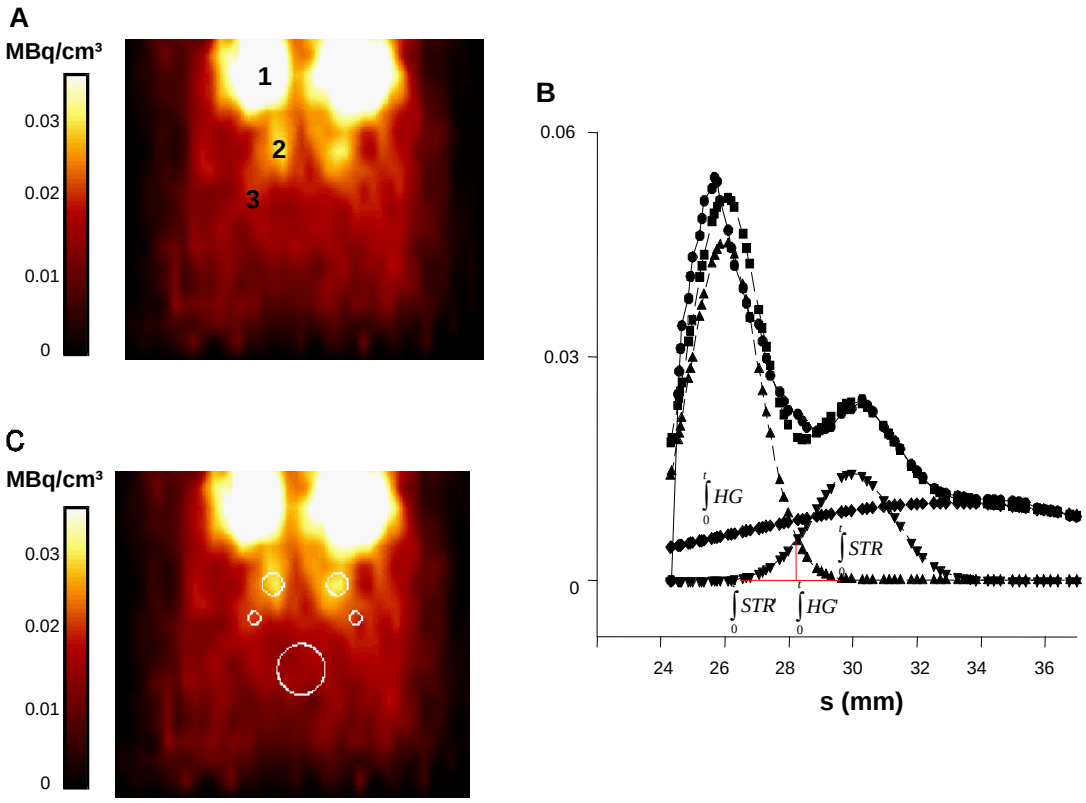

Fig. (1). (**A**) Characteristic transversal slice of a Sprague-Dawley rat head obtained with the PET camera. (**B**) In order to estimate the influence of the retroorbital radioactivity on the determination of striatal radioactivity concentrations, Gaussian model functions (triangles down) were fitted to the line activity profiles (circles) of both striata (1) and Harderian glands (2) of each side (right). After decomposition of the sum function into the three components "striatal" (diamonds), "retroorbital" (black squares), and "cortical radioactivity" (triangles up), the overlap ($\int_0^t STR / \int_0^t HG$ and $\int_0^t HG / \int_0^t STR$) between striatal and orbital curve was taken as a measure for spill-over. Cortical radioactivity (3) was used to estimate free and non-specific binding. For each animal, the mean cortical values are subtracted from striatal radioactivity concentrations as averaged over time frames four to six. (**C**) For the analysis of data according to the equilibrium distribution volume method, standard circular ROIs with diameters of 2.5 mm and 1.2 mm, respectively, were drawn around the centers of both striata and within the adjacent cortex of each side. Within the cerebellum, a region with a diameter of 5.5 mm was defined.

curves were generated by fitting the hyperbolic function $y = \frac{B_{max} x}{K_d + x}$ to the data set with x and y corresponding to the concentrations of free, [L], and bound radioligand, [LR], respectively. The standard errors (SE) of kinetic parameters derived by non-linear regression analysis represent functions of the degrees of freedom, the distance of the measured points from the curves, and the overall shape of the curves. We additionally report the coefficient of variation (%CV) as a measure of identifiability of the parameters. The goodness of fit was quantified by the coefficient of determination R^2. R^2 was computed by dividing the sum of squares of the vertical distances of the measured points from the best-fit curve by the sum of squares of the distances of the measured points from a horizontal line through the mean of all y-values. For linear regression analysis, the straight line function $y' = -\frac{1}{K_d} x' + \frac{B_{max}}{K_d}$ was fitted to Scatchard transformed data with x' and y' corresponding to [LR] and [LR]/[L], respectively. Thereby, the x-intercept of the Scatchard line represented B_{max}, while the slope equaled $-1/K_d$. Additionally, means and standard deviations of slope and Y-intercept are given. The goodness of fit was quantified by the coefficient of determination r^2. For statistical analysis, the overall shapes of the fitted saturation binding curves was compared using the F-test ($\alpha = 0.05$). The BPs of [^{18}F]FMB in the rat striatum after both non-linear and linear regression analysis were calculated by dividing B_{max} by K_d.

In order to assess, whether the rat cortex as measured with the TierPET was suitable as a REF, cerebellar molar concentration additionally were subtracted from cortical radioligand concentrations, and subjected to both non-linear and linear regression analysis.

Equilibrium distribution volume method. After summation of time frames 4 to 6, standard circular ROIs with diameters of 2.5 mm and 1.2 mm, respectively, were drawn around the centers of both striata and within the adjacent parietooccipital cortex of each side. Within the cerebellum, a circular region with a diameter of 5.5 mm was delineated (Fig. **1C**). Left and right striatal as well as cortical count rates were averaged. Partial-volume effects led to an underestimation of striatal radioactivity by approximately 60%, while spill-over determined as described above caused an overestimation by 5%; striatal count rates were corrected on the basis of these values [40]. For each animal, V_3'' was computed by dividing radioactivity counts in the ROI (striatum, parietooccipital cortex) by radioactivity counts in the REF (parietooccipitalcortex and cerebellum, respectively) and subtracting 1. The V_3'' values obtained for each animal were averaged, and standard deviations of the means (SD) were computed. Striatal V_3'' values obtained with either cortical or cerebellar reference tissue and striatal and cortical V_3'' values were compared using the paired t-test ($\alpha = 0.05$).

RESULTS

Decay corrected striatal radioactivity concentrations amounted to 30 ± 6 counts/pixel (mean ± SD) corresponding to 0.14 ± 0.04 MBq/cm³. After corrections for partial volume effect and spill-over, striatal count rates and radioactivity concentrations were 74 ± 14 counts/pixel and 0.35 ± 0.12 MBq/cm³, respectively.

Saturation binding analysis. Non-linear regression analysis of corrected striatal data with the cortical radioligand accumulation as concentration parameter yielded a K_d of 6.2 nM (SE: 3.8 nM, %CV: 61.3) and a B_{max} of 16 fmol/mg (SE: 4.7 fmol/mg; %CV: 29.4; Fig. **2A**). R^2 was 0.8. Regression analysis of the linearized data yielded K_d and B_{max} values of 5 nM and 15.3 fmol/mg, respectively (slope: -0.2 ± 0.1, Y-intercept: 3.0 ± 0.9 fmol/mg; inset of Fig. **2A**). The coefficient of determination r^2 was 0.4. BP values amounted to 2.6 ± 2.3 (non-linear regression analysis) and 3.1 ± 2.5 (linear regression analysis).

With the cerebellar radioligand accumulation as concentration parameter non-linear regression analysis yielded a K_d of 3.0 nM (SE: 2.1 nM, %CV: 70) and a B_{max} of 25.5 fmol/mg (SE: 9.1 fmol/mg; %CV: 35.7; Fig. **2B**). R^2 was 0.7. Regression analysis of the Scatchard plot yielded K_d and B_{max} values of 9.2 nM and 55.8 fmol/mg, respectively (slope: -0.11 ± 0.21, Y-intercept: 6.1 ± 2.6 fmol/mg; inset of Fig. **2B**). The coefficient of determination r^2 was 0.1. BP values were 8.4 ± 8.9 (non-linear regression analysis) and 6.1 ± 14.2 (linear regression analysis).

Fig. (**2C**) shows the saturation binding curves obtained with concentrations parameters derived from either cortical or cerebellar radioactivity accumulations in the same plot. Saturation binding curves significantly differed as to their overall shapes (F-test, $p < 0.0001$).

No reliable saturation binding curves could be obtained for cortical binding data (K_d: 7.2 nM, SE: 11.4 nM, %CV: 158; B_{max} : 27.14 fmol/mg, SE: 29.17 fmol/mg, %CV: 107; data not shown).

Equilibrium distribution volume method. V_3'' obtained with cortical and cerebellar reference tissue amounted to 2.2 ± 0.3 and 3.2 ± 0.6, respectively (paired t-test, $p_{two\text{-}tailed} < 0.0001$). For the cortex, a V_3'' of 0.29 ± 0.1 was obtained. V_3'' values differed significantly between cortex and striatum (paired t-test, $p_{two\text{-}tailed} < 0.0001$; data not shown).

DISCUSSION

In vivo saturation binding anaysis of striatal [^{18}F]FMB accumulation yielded BP values of 2.6 (non-linear regission analysis) and 3.1 (linear regression analysis) with cortical radioactivty as a measure of free and non-specifically bound radioligand. With a cerebellar REF, BP values amounted to 8.4 and 6.1, respectively. Thus, employment of the cortex instead of the cerebellum as REF led to a reduction of the BP by 50 to 70% dependent on the method of regression analysis. Accordingly, saturation binding curves obtained with cortex and cerebellum as measures of free and non-specific radioligand binding differed significantly.

With the equilibrium distribution volume method, mean striatal V_3'' values of 2.2 and 3.2 with cortical and cerebellar reference tissue, respectively, were obtained, corresponding to striatum to cortex and striatum to cerebellum ratios of 3.2 and 4.2. Thus, V_3'' as an equivalent of the striatal BP was reduced by ≈ 30%, when the cortex was used as a REF instead of the cerebellum. Accordingly, V_3'' values obtained

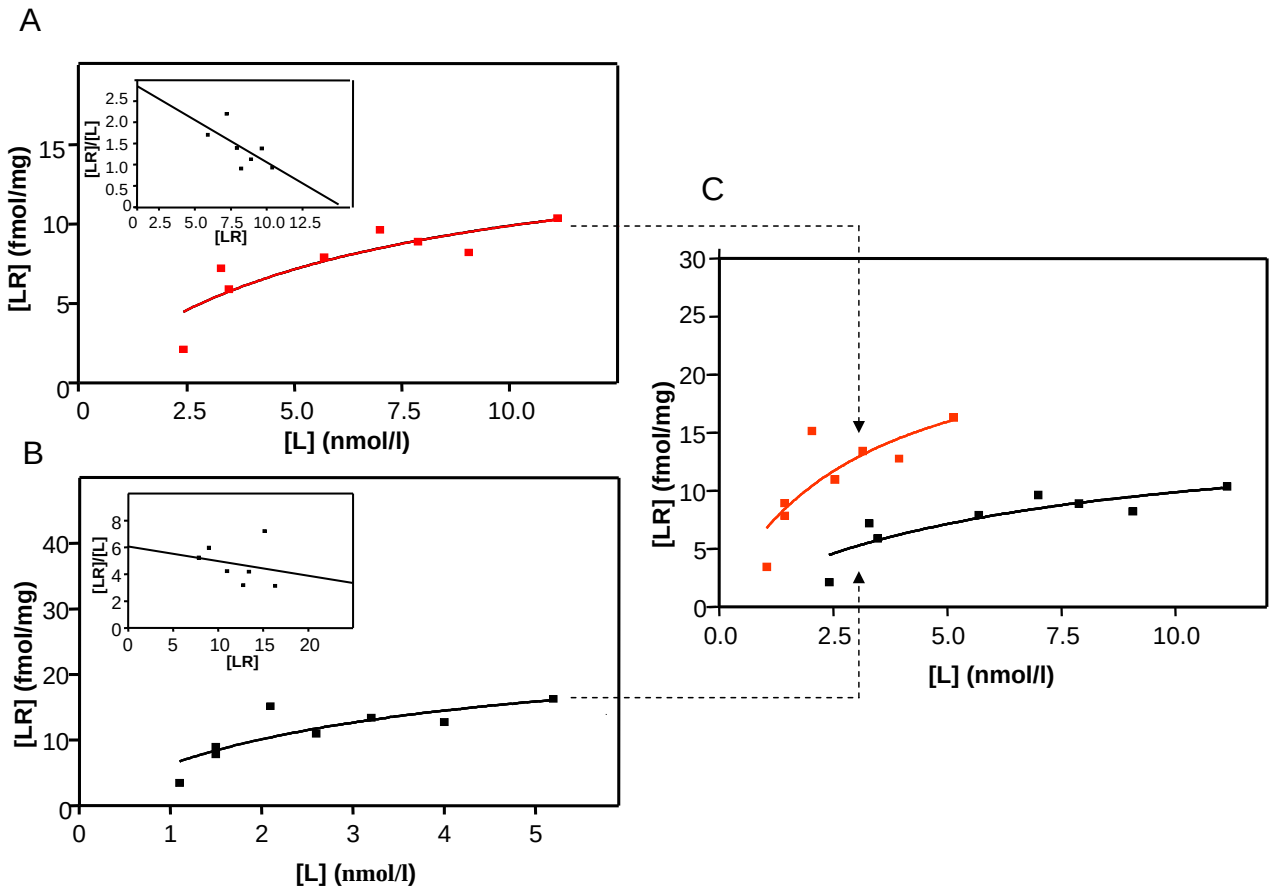

Fig. (2). (**A**) Non-linear regression analysis of [^{18}F]FMB binding to striatal dopamine D_2 receptors with the free radioligand concentration in the occipital *cortex* as concentration parameter. (**B**) Non-linear regression analysis of [^{18}F]FMB binding to striatal dopamine D_2 receptors with the free radioligand concentration in the *cerebellum* as concentration parameter. Binding data were acquired on a total of 8 Sprague-Dawley rats with a small animal PET. The insets show the linear regression analysis of Scatchard transformed data in each condition. (**C**) *In vivo* saturation binding curves with concentration parameters derived from either cortical or cerebellar radioactivity accumulations in the same plot. Saturation binding curves significantly differed as to their overall shapes (F-test, $p < 0.0001$).

with cortical and cerebellar reference tissue were found to be significantly different.

With *in vivo* saturation binding analysis, cortical [^{18}F]FMB binding could not be reasonably fitted. However, applying the equilibrium distribution volume method, a cortical V_3'' of 0.3 was obtained corresponding to a cortex to cerebellum ratio of 1.3. This value is indicative of a low though still existent amount of D_2 receptor binding in the rat parietal cortex, which is reflected by the results obtained from autoradiographic studies [34].

For *in vivo* saturation binding analyses with the concentration parameters derived from cortical and cerebellar radioactivity concentrations R^2 values of 0.8 and 0.7, respectively, were obtained, indicating in either case a reasonable goodness of fit of non-linear regression analysis. In contrast, with r^2 values of 0.4 and 0.1, respectively, the goodness of fit of linear regression analysis was poor. The %CV's for K_d and B_{max} values obtained with the concentration parameter derived from the cerebellum were higher (70% and 36%, respectively) than for K_d and B_{max} values obtained with the concentration parameter derived from the cortex (61% and 30%, respectively). This as well as the slightly higher R^2 value obtained for *in vivo* saturation binding analysis with a cortical concentration parameter implies that our method of estimating cortical radioactivity concentrations from Gaussian fits to line-activity profiles may be less prone to errors than the delineation of cerebellar reference regions without concurrent morphological imaging.

Interestingly, nonwithstanding the statistically significant differences between binding values obtained with cortical or cerebellar reference tissue, results obtained with both *in vivo* saturation binding analysis and equilibrium distribution volume method are in the same order of magnitude as previous ex vivo findings of Suehiro *et al*., who assessed ^{11}C(N-methyl)benperidol binding in mice and reported striatum to cerebellum and cortex to cerebellum ratios of 6.2 and 1.2 corresponding to V_3'' values of 5.2 and 0.2, respectively [44]. Similarly, *in vivo* measurements of [^{18}F]FMB binding in baboons yielded a striatum to cerebellum ratio of ≈ 4 at ≈ 35 min post-injection [41].

In a previous study, B_{max} and K_d values of [^{18}F]FMB were determined *in vitro* with the non-specific binding either estimated from joint incubation with the radioligand and a highly selective competitor or from cortical radioactivity concentrations as was done in the present evaluation of *in vivo* data [24]. With non-linear regression analysis, K_d and B_{max} amounted to 4.4 nM and 84.1 fmol/mg (subtraction of [^{18}F]FMB binding in the presence of raclopride) and 7.9 nM and 70.1 fmol/mg (subtraction of cortical radioactivity concentrations), respectively, thus yielding BP values of either 19.1 or 8.8. From this follows that the BP value as determined with *in vivo* saturation binding analysis in combination with a cerebellar REF and non-linear regression analysis provided the closest approximation to the BP determined with *in vitro* autoradiography as a gold standard. Still, however, values differ by a factor of 2.

In comparing *in vivo* and *in vitro* measurements, however, various issues should be considered: firstly, the exact determination of the anterioposterior stereotaxic coordinates of the PET slices is hampered, when no concurrent morphological imaging may be performed, as was the case in our investigation. Non-corresponding sectional planes between PET and autoradiography, thus, offer one explanation for the difference between receptor densities obtained *in vivo* and *in vitro*. Secondly, the applied partial-volume correction factor was estimated on the basis of phantom studies, and entered as a constant factor into the quantification of radioactivity values irrespective of the actual striatal diameters on the slices selected for ROI definition. If the striatal diameter had fallen below 2.5 mm, the used correction factor would have led to an underestimation of radioactivity concentration compared to autoradiography. This may have been the case, since the selection of slices was performed not only with respect to the localization of the striatal activity maxima but also with the intent to minimize spill-over form the adjacent retroorbital tissue. Thirdly, *in vivo* and *in vitro*, the mean free ligand concentration in tissue is assumed to be equal to the 'true' free ligand concentration in the vicinity of the binding sites. We do not know to which extent this assumption is violated in either case. *In vitro*, the 'true' free radioligand concentration may be influenced by the diffusion of molecules into the brain tissue, which - apart from external conditions such as temperature - in turn depends on the degree of cellular destruction in the cryosections. Moreover, in the *in vitro* experiment [24], no non-specifically bound portions of [^{18}F]FMB were present in the radioligand solution, and the free radioligand concentration as such entered into the saturation binding analysis possibly leading to an overestimation of specific binding.

In the *in vivo* saturation binding approach, accuracy depends on the correctness of the assumption that C_2 and C_2' may be pooled into one compartment. Actually, we derive [L], that is, both the free and the non-specifically bound radioligand concentration from either the cortical or the cerebellar tissue. Thus, in our approach, BP is given by $\frac{[LR]}{[L]} - 1$. As [L] corresponds to C_2 + C_2', the non-specifically-bound radioligand enters into the denominator in addition to the free radioligand concentration. Thus, the correctness of parameter estimation suffers from the fact, that the free fraction of radioligand in C_2, f_2, may not be accurately determined. Actually, with our method, we derive B_{max}' (= f_2B_{max}), and thus, consistently underestimate B_{max}.

Similarly, in the equilibrium distribution volume method applied in this investigation, a REF is employed for the estimation of V_2 + V_2' [27]. Hence, the occurrence of non-specifically bound radioligand in the REF may lead to similar underestimations of BP. Actually, instead of B_{max}/K_d, f_2B_{max}/K_d is obtained as an outcome measure. This, by the way, offers a further explanation for the fact, that the striatal V_3'' obtained with a cortical REF falls short of V_3'' obtained with cerebellar reference tissue. Matters are similar in the simplified reference tissue model [45]. A REF is used for the estimation of C_2 + C_2', and also here the portion of non-specifically bound radioligand may lead to underestimations of BP. As in the equilibrium distribution volume method, f_2B_{max}/K_d is obtained as an outcome measure.

In discussing possible errors of parameter estimation, their degree, however, should be viewed in relation to other error sources inherent to the method of *in vivo* PET imaging, such as spill-over and partial-volume effect. For the non-specific binding, moreover, holds that it is characterized by both tissue and radioligand properties, which are not assumed to vary over time or between subjects. Thus, f_2B_{max} and K_d, as well as f_2B_{max}/K_D, obtained with *in vivo* saturation binding analysis and simplified reference tissue model and equilibrium distribution volume method, respectively, can be considered to provide reasonable estimates of the receptor parameters in question. Thereby, the particular advantage of *in vivo* saturation binding analysis is the provision of B_{max}(') and K_d as separate values and direct measures of receptor density and affinity.

Taken together, findings show that for the quantitation of D_2 receptor binding in the rat striatum *in vivo* saturation binding analysis may be used as well as the equilibrium distribution volume method. Moreover, both cortex – especially the parietooccipital cortex, which was used in the present investigation – and cerebellum may be suitable as reference tissue with respect to striatal D_2 receptor binding. As to *in vivo* saturation binding analysis, both regions are likely to provide reasonable estimates of free and non-specific radioligand concentrations. However, the significant difference between binding values obtained with cortical and cerebellar tissues indicates that caution should be exerted in choosing the reference tissue with regard to the intended investigation. The cortex may be adequate in intra- or interindividual comparisons between varying experimental conditions. One example is the multiple investigation of the same animals in order to assess 6-hydroxydopamine-induced changes of D_2 receptor binding [25]. It is advisable, however, to select a region devoid of D_2 receptors such as the cerebellum, if the *in vivo* characterization of a novel D_2 receptor ligand is intended, which requires a more accurate quantification of the BP.

Thereby, it should be born in mind, that in our investigation, *in vivo* saturation binding analysis obtained with the concentration parameter obtained from cortical radioactivity was more robust compared to *in vivo* saturation binding analysis with cerebellar radioactivity as an estimate of free and non-specific binding, with the confinement, however, that this might have been due to our method of

deriving cortical radioactivity from Gaussian fits to line-activity profiles placed through Harderian glands, striatum and adjacent cortical tissue. This method was chosen, as it permitted to account for spill-over between the individual regions. In small animal investigation performed with higher resolving PET cameras analysis of line-activity profiles, probably, can be dispensed with. In addition, coregistration with CT images, which is state of the art now, will render possible a more exact definition of ROIs and REFs improving the exactitude of parameter estimation with both (non-linear) regression analysis of saturation binding curves and the equilibrium distribution volume method.

ACKNOWLEDGEMENTS

This work was supported by a grant from the 'Forschungskommission' of the Faculty of Medicine, Heinrich-Heine-University, Düsseldorf, Germany. The authors acknowledge Dr. Simone Weber from the Central Laboratory for Electronics and Dr. Karl Hamacher from the Institute of Nuclear Chemistry (Forschungszentrum Jülich GmbH, Jülich, Germany) for their contributions to the experiments.

REFERENCES

[1] Nikolaus S, Beu M, Wirrwar A, Vosberg H, Müller HW, Larisch R. The contribution of small animal positron emission tomography to the neurosciences – a critical evaluation. Rev Neurosci 2004; 15: 131-56.

[2] Nikolaus S, Larisch R, Beu M, *et al*. Investigating the dopaminergic synapse *in vivo*. II. Molecular imaging studies in small laboratory animals. Rev Neurosci 2007; 18: 473-505.

[3] Slifstein M, Laruelle M. Models and methods for derivation of *in vivo* neuroreceptor parameters with PET and SPECT reversible radiotracers. Nucl Med Biol 2001; 28: 595-608.

[4] Nikolaus S, Wirrwar A, Klimke A, *et al*. State-of-the-art in high-resolution imaging of small animals with PET and SPECT. In: Mohan RM, Ed. Research Advances in Nuclear Medicine. Kerala, India: Global Research Networks 2002; Vol. 1: pp. 13-29.

[5] Ogawa O, Umegaki H, Ishiwata K, *et al*. *In vivo* imaging of adenovirus-mediated over-expression of dopamine D_2 receptors in rat striatum by positron emission tomography. Neuroreport 2000; 11: 743-8.

[6] Tsukada H, Kreuter J, Maggos CE, *et al*. Effects of binge pattern cocaine administration on dopamine D_1 and D_2 receptors in the rat brain: an *in vivo* study using positron emission tomography. J Neurosci 1996; 16: 7670-77.

[7] Unterwald EM, Tsukada H, Kakiuchi T, Kosugi T, Nishiyama S, Kreek MJ. Use of positron emission tomography to measure the effects of nalmefene on D_1 and D_2 dopamine receptors in rat brain. Brain Res 1997; 775: 183-8.

[8] Maggos CE, Tsukada H, Kakiuchi T, *et al*. Sustained withdrawal allows normalization of *in vivo* [^{11}C]methylspiperone dopamine D_2 receptor binding after chronic binge cocaine: a positron emission tomography study in rats. Neuropsychopharmacology 1998; 19: 146-53.

[9] Nguyen TV, Brownell AL, Chen YCI, *et al*. Detection of the effects of dopamine receptor sensitivity using pharmacological MRI and correlations with PET. Synapse 2000; 36: 57-65.

[10] Suzuki M, Hatano K, Sakiyama Y, Kawasumi J, Kato T, Ito K. Age-related changes of dopamine D_1-like and D_2-like receptor binding in the F344/N rat striatum revealed by positron emission tomography and *in vitro* receptor autoradiography. Synapse 2001; 41: 285-93.

[11] Le Masurier M, Houston G, Cowen P, Grasby P, Sharp T, Hume S. Tyrosine-free amino acid mixture attenuates amphetamine-induced displacement of [11C]raclopride in striatum *in vivo*: a rat PET study. Synapse 2004; 51: 151-7.

[12] Honer M, Bruhlmeier M, Missimer J, Schubiger AP, Ametamey SM. Dynamic imaging of striatal D2 receptors in mice using quad-HIDAC PET. J Nucl Med 2004; 45: 464-70.

[13] Schiffer WK, Volkow ND, Fowler JS, Alexoff DL, Logan J, Dewey SL. Therapeutic doses of amphetamine or methylphenidate differentially increase synaptic and extracellular dopamine. Synapse 2006; 59: 2432-51.

[14] Hume SP, Lammertsma AA, Myers R, *et al*. The potential of high-resolution positron emission tomography to monitor striatal dopaminergic function in rat models of disease. J Neurosci Method 1996; 67: 103-12.

[15] Torres EM, Fricker RA, Hume SP, *et al*. Assessment of striatal graft viability in the rat *in vivo* using a small diameter PET scanner. Neuroreport 1995; 6: 2017-21.

[16] Fricker RA, Torres EM, Hume SP, *et al*. The effects of donor stage on the survival and function of embryonic striatal grafts in the adult rat brain. II. Correlation between positron emission tomography and reaching behaviour. Neuroscience 1997; 79: 711-21.

[17] Opacka-Juffry J, Ashworth S, Ahier RG, Hume SP. Modulatory effects of L-DOPA on D_2 dopamine receptors in rat striatum, measured using *in vivo* microdialysis and PET. J Neural Transm 1989; 105: 349-64.

[18] Araujo DM, Cherry SR, Tatsukawa KJ, Toyokuni T, Kornblum HI. Deficits in striatal dopamine D_2 receptors and energy metabolism detected by *in vivo* microPET imaging in a rat model of Huntington's disease. Exp Neurol 2000; 166: 287-97.

[19] Umegaki H, Ishiwata K, Ogawa O, *et al*. *In vivo* assessment of adenoviral vector-mediated gene expression of dopamine D_2 receptors in the rat striatum by positron emission tomography. Synapse 2002; 43: 195-200.

[20] Ishiwata K, Ogi N, Hayakawa N, *et al*. Positron emission tomography and ex vivo and *in vitro* autoradiography studies on dopamine D2-like receptor degeneration in the quinolinic acid-lesioned rat striatum: comparison of [11C]raclopride, [11C]nemonapride and [11C]N-methylspiperone. Nucl Med Biol 2002; 29: 307-16.

[21] Houston GC, Hume SP, Hirani E, Goggi JL, Grasby PM. Temporal characterisation of amphetamine-induced dopamine release assessed with [11C]raclopride in anaesthetised rodents. Synapse 2004; 51: 206-12.

[22] Morris ED, Yoder KK, Wang C, *et al*. ntPET: a new application of PET imaging for characterizing the kinetics of endogenous neurotransmitter release. Mol Imaging 2005; 4: 473-89.

[23] Inaji M, Okauchi T, Ando K, *et al*. Correlation between quantitative imaging and behavior in unilaterally 6-OHDA-lesioned rats. Brain Res 2005; 1064: 136-45.

[24] Nikolaus S, Larisch R, Beu M, *et al*. *In vivo* measurement of D_2 receptor density and affinity for ^{18}F-(3-N-methyl) benperidol in the rat striatum with a PET system for small laboratory animals. J Nucl Med 2003; 44: 618-24.

[25] Nikolaus S, Larisch R, Beu M, Forutan F, Vosberg H, Müller-Gärtner HW. Bilateral increase in striatal dopamine D_2 receptor density in the 6-hydroxydopamine-lesioned rat: a serial *in vivo* investigation with small animal PET. Eur. J Nucl Med 2003; 30: 390-5.

[26] Nikolaus S, Beu M, Vosberg H, Müller HW, Larisch R. Quantitative analysis of dopamine D_2 receptor kinetics with small animal positron emission tomography. Method Enzymol 2004; 385: 228-39.

[27] Laruelle M, van Dyck C, Abi-Dargham A, *et al*. Compartmental modeling of iodine-123-iodobenzofuran binding to dopamine D2 receptors in healthy subjects. J Nucl Med 1994; 35: 743-54

[28] Rinne UK, Laihinen A, Rinne JO, *et al*. Positron emission tomography demonstrates dopamine D2 receptor supersensitivity in the striatum of patients with early Parkinson's disease. Mov Disord 1990; 4: 55-9.

[29] Antonini A, Leenders KL, Vontobel P, *et al*. Complementary PET studies of striatal neuronal function in the differential diagnosis between multiple system atrophy and Parkinson's disease. Brain 1997; 120: 2187-95.

[30] Larisch R, Klimke A, Vosberg H, *et al*. *In vivo* evidence for the involvement of dopamine-D2 receptors in striatum and anterior cingulate gyrus in major depression. Neuroimage 1997; 5: 251-60.

[31] Brucke T, Podreka I, Angelberger P, *et al*. Dopamine D2 receptor imaging with SPECT: studies in different neuropsychiatric disorders. J Cereb Blood Flow Metab 1991; 11: 220-8.

[32] Knudsen GM, Karlsborg M, Thomsen G, *et al*. Imaging of dopamine transporters and D2 receptors in patients with

Parkinson's disease and multiple system atrophy. Eur J Nucl Med Mol Imaging 2004; 31: 1631-8.

[33] Plotkin M, Amthauer H, Klaffke S, *et al*. Combined 123I-FP-CIT and 123I-IBZM SPECT for the diagnosis of parkinsonian syndromes: study on 72 patients. J Neural Transm 2005; 112: 677-92.

[34] Kessler RM, Mason NS, Votaw JR, *et al*. Visualization of extrastriatal dopamine D_2 receptors in the human brain. Eur J Pharmacol 1992; 223: 105-7.

[35] Moerlein SM, Banks WR, Parkinson D. Production of fluorine-18 labeled (3-N-methyl)benperidol for PET investigation of cerebral receptor binding. Appl Radiat Isot 1992; 43: 913-7.

[36] Hamacher K, Hamkens W. Remote controlled one-step production of ^{18}F labeled butyrophenone neuroleptics exemplified by the synthesis of n.a.c. [^{18}F]N-methylspiperone. Appl Radiat Isot 1995; 46: 911-6.

[37] Moerlein SM, Perlmutter JS, Welch MJ. Specific, reversible binding of [^{18}F]benperidol to baboon D_2 receptors: PET evaluation of an improved ^{18}F-labeled ligand. Nucl Med Biol 1995; 22: 809-15.

[38] Digenis GA, Vincent SH, Kook CS, Reiman RE, Russ GA, Tilbury RS. Tissue distribution studies of [^{18}F]haloperidol, [^{18}F]-β-[4-fluorobenzoyl)propionic acid, and [^{82}Br]bromperidol by external scintigraphy. J Pharm Sci 1981; 70: 985.

[39] Weber S, Terstegge A, Herzog H, *et al*. The design of an animal PET: flexible geometry for achieving optimal spatial resolution or high sensitivity. IEEE Trans Med Imaging 1997; 16: 684-98.

[40] Nikolaus S, Larisch R, Beu M, Vosberg H, Müller-Gärtner HW. Imaging of striatal dopamine D_2 receptors with a PET system for small laboratory animals in comparison with storage phosphor autoradiography: a validation study with [^{18}F](3-N-methyl)benperidol. J Nucl Med 2001; 42: 1691-6.

[41] Moerlein SM, Perlmutter, JS, Markham J, Welch MJ. *In vivo* kinetics of [^{18}F](N-methyl)benperidol: a novel PET tracer for assessment of dopaminergic D_2-like receptor binding. J Cereb Blood Flow Metab 1997; 17: 833-45.

[42] Paxinos G, Watson C. The rat brain in stereotaxic coordinates. Sydney: Academic Press 1986.

[43] Ito H, Hietala J, Blomqvist G, Halldin C, Farde L. Comparison of the transient equilibrium and continuous infusion method for quantitative PET analysis of [^{11}C]raclopride binding. J Cereb Blood Flow Metab 1998; 18: 941-50.

[44] Suehiro M, Dannals RF, Scheffel U, *et al*. *In vivo* labeling of the dopamine D_2 receptor with N-^{11}C-methyl-benperidol. J Nucl Med 1990; 31: 2015-21.

[45] Lammertsma AA, Hume SP. Simplified reference tissue model for PET receptor studies. Neuroimage 1996; 4: 153-8.

Received: April 23, 2009 Revised: May 26, 2009 Accepted: June 15, 2009